NIES-GOSAT2-ALG-20191008-011-02

GOSAT-2 TANSO-FTS-2 L2 Pre-processing Algorithm Theoretical Basis Document

August 2022

National Institute for Environmental Studies
GOSAT-2 Project

YOSHIDA Yukio[1)]

1) Center for Global Environmental Research, National Institute for Environmental Studies

Revision History

Version	Revised on	Page	Description
00	Nov. 2020	-	-
01	Mar. 2021	p.28	Modified the formula in 4.4.3
02	Aug. 2022	p.10, p.11, p.12, p.25	Modified the reference data name
		p.25	Added description in 4.4 (b)

※The affiliations are as of version 00.

CONTENTS

1. Introduction

This Algorithm Theoretical Basis Document (ATBD) describes the pre-processing algorithm which is necessary for TANSO-FTS-2 L2 processing by using observed radiance spectra from TANSO-FTS-2 (TANSO-FTS-2 L1B Product) onboard GOSAT-2.

1.1 Scope of the Algorithm

Figure 1.1-1 shows the whole processing flow of GOSAT-2 data analysis. The scope of application in this ATBD is the yellow-colored part in the figure.

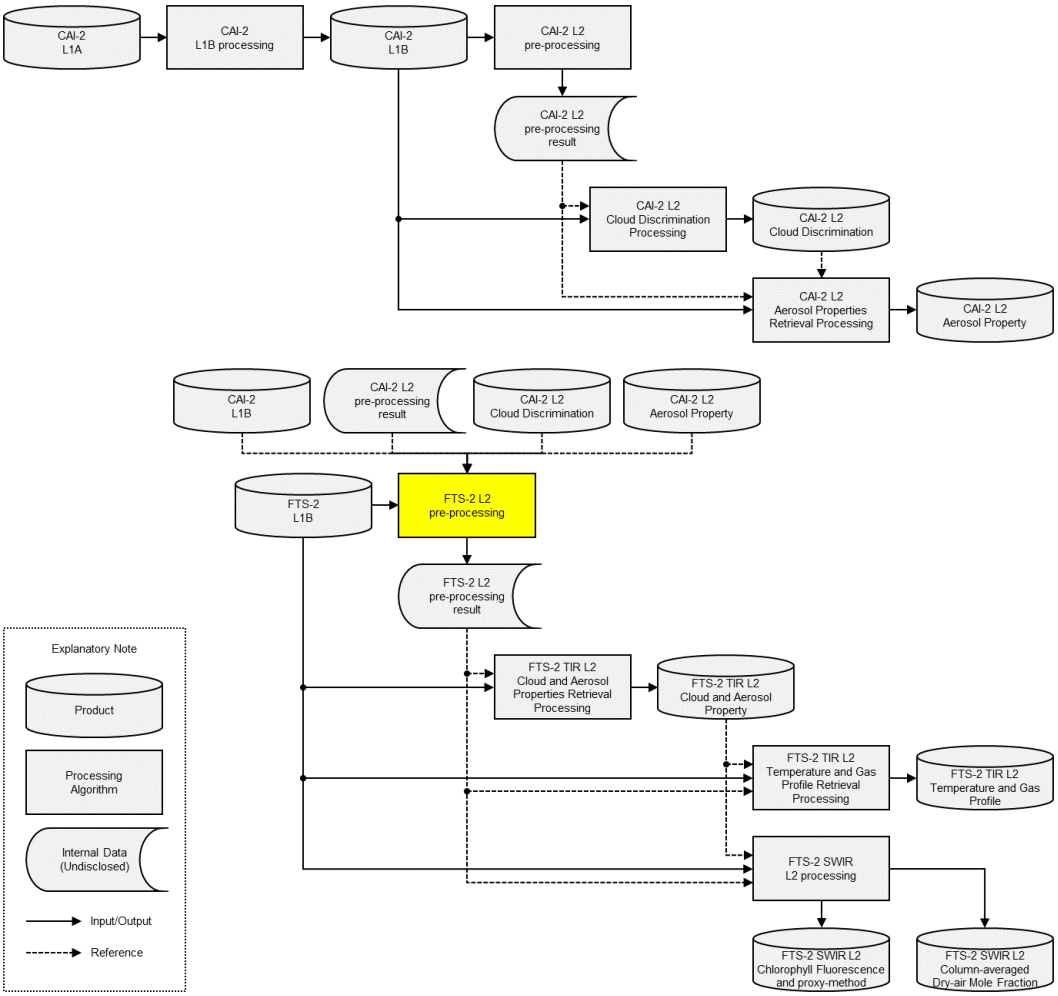

Figure 1.1-1. The scope of the algorithm described in this ATBD in the processing flow of GOSAT-2 data analysis.

1.2 Related Documents

Related documents of the ATBD are as follows.

(1) Algorithm Theoretical Basis Document for Greenhouse gases Observing SATellite-2 (GOSAT-2)

(2) GOSAT-2/TANSO-FTS-2 Level 1 Product Description Document

(3) GOSAT-2 TANSO-CAI-2 L1B Processing Algorithm Theoretical Basis Document

(4) GOSAT-2 TANSO-CAI-2 L2 Pre-processing Algorithm Theoretical Basis Document

(5) GOSAT-2 TANSO-CAI-2 L2 Cloud Discrimination Processing Algorithm Theoretical Basis Document

(6) GOSAT-2 TANSO-CAI-2 L2 Aerosol Properties Retrieval Processing Algorithm Theoretical Basis Document

(7) NIES GOSAT-2 Product File Format Descriptions (Product edition)

- Vol. 1: GOSAT-2 TANSO-CAI-2 L1B Product
- Vol. 2: GOSAT-2 TANSO-CAI-2 L2 Cloud Discrimination Product
- Vol. 3: GOSAT-2 TANSO-CAI-2 L2 Aerosol Properties Product

2. Background

2.1 Overview of Observation Instruments

GOSAT-2 carries two sensors: Thermal And Near-infrared Sensor for carbon Observation-Fourier Transform Spectrometer 2 (TANSO-FTS-2, hereafter "FTS-2") and TANSO-Cloud and Aerosol Imager 2 (TANSO-CAI-2, hereafter "CAI-2"). FTS-2 is a Fourier transform spectrometer which has three bands in the short wavelength infrared (SWIR) regions and two bands in the thermal infrared (TIR) regions. It observes any points up to ±40 degrees in the along track (AT) direction and ±35 degrees in the cross track (CT) direction, within 15.8 mrad of the instantaneous field of view (IFOV) (equivalent to a circle with a diameter of about 9.7 km at the nadir point of the satellite.), by using the two-axis pointing control mechanisms. CAI-2 is an electronic scanning imager which has each five bands of forward and backward viewing (±20°) from the nadir point of the satellite in the along track direction from ultraviolet to short wavelength infrared bands, 10 bands in total. It observes the 920-km field of view (FOV) in the cross track direction with spatial resolution of 0.46 km or 0.92 km. The specifications of FTS-2 and CAI-2 are summarized in Table 2.1-1 and Table 2.1-2, respectively.

The FTS-2 TIR is operated in both day side and night side while the operations of the FTS-2 SWIR and CAI-2 are limited to the day side area on the ground.

Table 2.1-1. Specifications of TANSO-FTS-2.

	Band 1	Band 2	Band 3	Band 4	Band 5
Polarization observation	Yes	Yes	Yes	No	No
Spectral coverage [cm^{-1}]	12950 - 13250	5900 - 6400	4200 - 5200	1188 - 1800	700 - 1188
FWHM of the instrument line shape function	< 0.4 cm^{-1}	< 0.27 cm^{-1}	< 0.27 cm^{-1}	< 0.27 cm^{-1}	< 0.27 cm^{-1}
Sampling step	< 0.2 cm^{-1}	< 0.2 cm^{-1}	< 0.2 cm^{-1}	< 0.2 cm^{-1}	< 0.2 cm^{-1}
Interval time of data acquisition	Approx. 4.67 sec. (Time required for interferogram acquisition: 4.024 sec.)				
IFOV	15.8 mrad (Diameter projected on the earth's surface at the nadir point of the satellite: approx. 9.7 km)				
FOV	±40° (Along track direction), ±35° (Cross track direction)				

Table 2.1-2. Specifications of TANSO-CAI-2.

	Band 1 / 6	Band 2 / 7	Band 3 / 8	Band 4 / 9	Band 5 / 10
Optical Tube	Tube 1	Tube 2	Tube 3	Tube 4	Tube 5
Viewing direction	Forward viewing (+20° in AT direction) / Backward viewing (-20° in AT direction)				
Center wavelength [μm]	0.343 / 0.380	0.443 / 0.550	0.674	0.869	1.63
Wavelength width [μm]	< 0.02	< 0.02	< 0.02	< 0.02	< 0.09
Resolution	0.46 km				0.92 km
Effective pixels	2048				958
Swath	920 km				

2.2 FTS-2 L2 Pre-processing

As shown in Figure 1.1-1, FTS-2 has three types of L2 processing: FTS-2 TIR L2 cloud and aerosol properties retrieval processing, FTS-2 TIR L2 temperature and gas concentration profile retrieval processing, and FTS-2 SWIR L2 processing. FTS-2 L2 pre-processing sets information commonly used in multiple L2 processing, such as the vertical profiles of temperature and gas concentrations used in radiative transfer calculation included in L2 processing. Information that is more efficient to be set in FTS-2 L2 pre-processing is also set in FTS-2 L2 pre-processing although it is used only in individual processing.

3. Input and Output Data

3.1 Input Data

The input data for FTS-2 L2 pre-processing are FTS-2 L1B Product. FTS-2 L1B Product consists of “Common file” that stores information common to SWIR and TIR, “SWIR file” that stores SWIR information, and “TIR file” that stores TIR information. One scene data of FTS-2 L1B Product is defined as one span data divided one-revolution data into four, starting at ascending node. Scene 01 stores data from ascending node to the end of night side observation. Scene 02 stores data from the start of day side observation to descending node. Scene 03 stores data from descending node to the end of day side observation. Scene 04 stores data from the start of night side observation to next ascending node. The place where day side observation and night side observation are switched depends on season. FTS-2 L2 pre-processing uses the SWIR file for day side observation and the TIR file for night side observation. Table 3.1-1 shows the list of input data for FTS-2 L2 pre-processing.

Table 3.1-1. Dataset of FTS-2 L1B for FTS-2 L2 pre-processing.

Dataset name	Explanation	Unit
SoundingAttribute		
numSoundings	Number of observation data stored in files.	
observationTime	FTS-2 observation time. The central time of interferogram acquisition time of 4.024 sec. is stored.	
QualityInfo		
SNR [1)]	Simplified calculated SNR.	
ProcessingParameters		
alignmentMatrix	Coordinate transformation matrix converting from FTS-2 optical axis coordinate system to satellite-fixed coordinate system.	
SatelliteGeometry		
satPos_ECR	Satellite position in ECR at observation time.	km
satVel_ECR	Satellite velocity in ECR at observation time.	km/s
satToECR_Matrix	Coordinate transformation matrix converting from satellite-fixed coordinate system to ECR coordinate system.	
SolarGeometry		
solarPos_ECR	Apparent solar position in ECR at observation time.	km
solarVel_ECR	Apparent solar velocity in ECR at observation time.	km/s
PointingGeometry		
pointingAT	The motor rotation angle around AT axis at observation time.	deg.
pointingCT	The motor rotation angle around CT axis at observation time.	deg.
viewVector	Viewing vector in the satellite coordinate system at observation time.	
SoundingData		
WavenumberInfo		
numWN [1)]	Number of spectrum data.	
beginWN [1)]	Beginning wavenumbers of spectrum data.	cm^{-1}
deltaWN [1)]	Interval of wavenumber of spectrum data.	cm^{-1}
RawSpectrum		
band3P [1)]	Band 3P spectral data before sensitivity correction.	V/cm^{-1}
band3S [1)]	Band 3S spectral data before sensitivity correction.	V/cm^{-1}

1) Used only for day side observation.

3.2 Output Data

Table 3.2-1 shows the output data that is carried over to the subsequent FTS-2 L2 processing as a result of FTS-2 L2 pre-processing. All the output data listed here are not necessarily used in each subsequent FTS-2 L2 processing, and the usage is different for each FTS-2 L2 processing. For details, see each ATBD for FTS-2 L2 processing.

Table 3.2-1. Output data for FTS-2 L2 pre-processing.

Classification	Output data
FTS-2 observation geometry	Longitude [deg.], latitude [deg.], and elevation [m] after Ortho-correction with respect to the center of FTS-2 IFOV, and FTS-2 IFOV-area and extended IFOV-area (36 points each). Solar zenith angle [deg.] and azimuth angle [deg.], satellite zenith angle [deg.] and azimuth angle [deg.], and angle between direction of specular reflection and viewing direction [deg.] with respect to the center of FTS-2 IFOV after Ortho-correction. Angle between radiative transfer reference plane and scan mirror reflection reference plane [deg.], incident angle to scan mirror [deg.], angle between scan mirror reflection reference plane and FTS-2 detector reference plane [deg.], angle between polarization plane of observation light and radiative transfer reference plane [deg.]. Doppler velocity for the sun and the satellite [m/s].

Classification	Output data
Surface data	Surface temperature [K], surface pressure [hPa], surface wind speed (east-west wind, north-south wind) [m/s], and variance of surface wind speed [$(m/s)^2$] at the center of FTS-2 IFOV. Total number of grid points, number of effective grid points, average, standard deviation, and mode within FTS-2 IFOV-area for digital elevation model data [m], NDVI data, CAI-2 NDVI data, snow and ice data (MODIS), sea surface temperature data [K] (MODIS), and surface emissivity. Total number of grid points and number of grid points by category within FTS-2 IFOV-area for land/sea mask data and land cover data. Total number of grid points and number of grid points by category within FTS-2 IFOV-area for sea ice data (MODIS), and number of effective grid points, average, standard deviation, and mode within FTS-2 IFOV-area for sea ice temperature data [K] (MODIS). Sea surface temperature data [K] (NOAA), sea ice data (NSIDC), and sea ice concentration data [%] (NSIDC) at the center of FTS-2 IFOV.
Atmospheric data	Vertical profiles of pressure [hPa], temperature [K], geopotential height [m], east-west wind [m/s], north-south wind [m/s], relative humidity [%], potential vorticity [K m^2/kg/s], and gravitational acceleration [m/s^2], and tropopause height [m], which are interpolated in time and space to FTS-2 observation time and the center of IFOV. The number of layers in each vertical profile is based on the source data.
Gas concentration data [1)]	Vertical profiles of concentrations [ppm] and variance-covariance matrix [ppm^2] of H_2O, CO_2, O_3, N_2O, CO, CH_4, which are interpolated in time and space to FTS-2 observation time and the center of IFOV. The number of layers in each vertical profile and surface pressure [hPa] are based on the source data.

Classification	Output data
Aerosol data	Aerosol mass mixing ratio profile [kg/kg] which is interpolated in time and space to FTS-2 observation time and the center of IFOV. The number of layers of vertical profile and the type of aerosol are based on the source data. Total number of pixels and number of effective pixels within FTS-2 IFOV-area in each viewing direction for CAI-2 L2 Aerosol Property Product, as well as corresponding average, standard deviation, and mode values by band for aerosol optical thickness by particle size, single-scattering albedo, and Angstrom exponent. [2)]
Cloud condition within FTS-2 IFOV [2)]	Total number of pixels, number of sea pixels, number of effective sea pixels within FTS-2 extended IFOV-area in each viewing direction for CAI-2 L1B Product, as well as corresponding average, standard deviation, and mode values by band for radiance of sea pixels [$W/m^2/str/\mu m$]. Total number of pixels, number of sea pixels, number of effective pixels, number of pixels by range of overall clear confidence level, and number of pixels by range of Cone Angle for sea pixels within FTS-2 extended IFOV-area in each viewing direction for CAI-2 L2 Cloud Discrimination Product. Difference between observation time of CAI-2 pixel nearest to the center of FTS-2 IFOV and FTS-2 observation time [sec.]. Cloud determination result by CAI-2 L1B Product and viewing direction used for the determination. Cloud determination result by CAI-2 L2 Cloud Discrimination Product, viewing direction used for the determination, cloud coverage within FTS-2 IFOV-area, and index corresponding to minimum Cone Angle for sea pixels. Cloud determination result of FTS-2 2 μm band by polarization component, number of wavenumber points of spectral data used for the determination, and average and standard deviation of radiance normalized with noise level.

1) Unless otherwise specified, “dry-air mole fraction” is called “gas concentration”.

2) Valid values are output only for day side observation.

3.3 Reference Data

Table 3.3-1 shows reference data used for FTS-2 L2 pre-processing. The details can be referred in each sub-section of this section. Note that the information of source data is as of October 2020.

Table 3.3-1. Reference data used for FTS-2 L2 pre-processing.

Reference data	Main reference items
Digital elevation model data	Elevation
Geoid height data	Geoid height
Global land/sea flag	Land/sea flag
JRA-55	Atmospheric data, surface data, O_3 concentration profile, etc.
Variance-covariance matrix (JRA-55)	Variance-covariance matrix of atmospheric data, surface data, O_3 concentration profile, etc.
NICAM-TM	CO_2 concentration profile, CH_4 concentration profile
Variance-covariance matrix (NCIAM-TM)	Variance-covariance matrix of CO_2 concentration profile, CH_4 concentration profile
ACTM	N_2O concentration profile (daily)
Variance-covariance matrix (ACTM)	Variance-covariance matrix of N_2O concentration profile
CO climatological value	CO concentration profile
Variance-covariance matrix (CO climatological value)	Variance-covariance matrix of CO concentration profile
SPRINTARS	Aerosol mass mixing ratio profile
MODIS L3 MYD11A1	Surface emissivity (daily)
MODIS L3 MCD12Q1	Land cover (daily)
MODIS L3 MYD13Q1	NDVI (16-day)
MODIS L3 MYD10C1	Snow cover (daily)
MODIS L3 (SST)	Sea surface temperature
MODIS L3 MYD29P1D/1N	Sea ice (daily)
NOAA OISST (AVHRR-Only)	Sea surface temperature
NSIDC Data Set ID: G02135	Sea ice index
NSIDC Data Set ID: NISE	Snow and ice
CAI-2 L1B Product	Radiance in each band of CAI-2
CAI-2 L2 pre-processing result (surface albedo)	Surface albedo for each viewing direction obtained by CAI-2 L2 pre-processing

Reference data	Main reference items
CAI-2 L2 Cloud Discrimination Product	Overall clear confidence level for each viewing direction, etc.
CAI-2 L2 Aerosol Property Product	Aerosol optical thickness, Angstrom exponent, etc.

3.3.1 Digital elevation model data

Data obtained by combining multiple DEM data and processing the spatial resolution into a 15-second mesh, which is almost the same as the spatial resolution of CAI-2. The data used and use range are as follows:

ALOS DEM V2.1	60 degrees north ~ 60 degrees south (excluding some islands areas)
MODIS DEM	60 degrees north ~ 90 degrees north (excluding Greenland)
NSIDC DEM	60 degrees south ~ 90 degrees south
GTOPO30	Greenland
ASTER GDEM V2	Islands area
SRTM DEM	Islands area

3.3.2 Geoid height data

Files containing EGM96 geoid data with a spatial resolution of 15 minutes mesh. The data can be obtained from the National Geospatial-Intelligence Agency (https://earth-info.nga.mil/GandG/update/index.php?action=home).

3.3.3 Global land/sea flag

Files containing the discrimination of land and sea with a spatial resolution of 15 seconds mesh which is almost the same as that of CAI-2. This file is commonly used for CAI-2 and FTS-2 processing.

3.3.4 JRA-55 | 02

Among the Japanese 55-year Reanalysis (JRA-55) by the Japan Meteorological Agency, the following data are used.

(1) Isentropic analysis fields (anl_isentrop)
- Pressure, potential vorticity

(2) Model level analysis fields (anl_mdl)
- Geopotential height, temperature, u-component of wind, v-component of wind, specific humidity

(3) Surface analysis fields (anl_surf)

－ Pressure, temperature, u-component of wind, v-component of wind

(4) Isobaric forecast fields (fcst_p125)

－ Ozone mixing ratio

The JRA-55 data files are in GRIB1 format and can be obtained from the collaborative organizations which are listed on the webpage of JMA Data Dissemination System (JDDS, https://jra.kishou.go.jp/JRA-55/index_en.html). 02

3.3.5 Variance-covariance matrix (JRA-55)

Monthly variance-covariance matrices generated based on the JRA-55 data. The variance-covariance matrices of the following parameters for each model grid are calculated. 02

(1) Vertical profile of water vapor concentration

The specific humidity q of the model level analysis fields in Subsection 3.3.4 (2) is converted to dry-air mole fraction C_{H2O}, and the variance-covariance matrix is calculated.

$$C_{H2O} = \frac{q}{1-q}\frac{n_{dry}}{n_{H2O}} \tag{3.3.4-1}$$

where n_{dry} and n_{H2O} are the average molar mass of dry air and the molar mass of water vapor, respectively.

(2) Vertical profile of ozone concentration

The ozone mass mixing ratio w_{O3} of the isobaric forecast fields in Subsection 3.3.4 (4) is converted to the dry-air mole fraction C_{O3}, and the variance-covariance matrix is calculated.

$$C_{O3} = w_{O3}\frac{n_{dry}}{n_{O3}} \tag{3.3.4-2}$$

where n_{O3} is the molar mass of ozone.

(3) Surface wind speed

The wind speed V is calculated from the u-component of wind V_u and the v-component of wind V_v of the surface analysis fields in Subsection 3.3.4 (3), and the variance is calculated.

$$V = \sqrt{V_u^2 + V_v^2} \tag{3.3.4-3}$$

3.3.6 NICAM-TM

The vertical profiles of carbon dioxide and methane concentrations using the atmospheric

transport model NICAM-TM. JRA-55 is used as the meteorological field for the transport calculation. The calculation is performed in NIES.

3.3.7 Variance-covariance matrix (NICAM-TM)

The respective monthly variance-covariance matrices of the vertical profiles of carbon dioxide and methane concentrations generated based on the NICAM-TM data in Subsection 3.3.6. The variance-covariance matrix for the vertical profile of each gas concentration is calculated for each model grid.

3.3.8 ACTM

The vertical profile of nitrous oxide concentration using the atmospheric transport model ACTM. The data files are in GTOOL3 format and are provided by collaborating researchers belonging to the Meteorological Research Institute.

3.3.9 Variance-covariance matrix (ACTM)

The monthly variance-covariance matrix of the vertical profile of nitrous oxide concentration generated based on the ACTM data in Subsection 3.3.8. The variance-covariance matrix for the vertical profile of nitrous oxide concentration is calculated for each model grid.

3.3.10 CO climatological value

The monthly climatological value of the vertical profile of carbon monoxide generated based on the atmospheric chemical transport model MOZART data. The monthly mean vertical profile of carbon monoxide concentration is calculated for each model grid.

The source MOZART data files are in netCDF format and can be obtained from NCAR (https://www.acom.ucar.edu/wrf-chem/mozart.shtml).

3.3.11 Variance-covariance matrix (CO climatological value)

The monthly variance-covariance matrix of the vertical profile of carbon monoxide concentration generated based on the atmospheric chemical transport model MOZART data. The variance-covariance matrix for the vertical profile of carbon monoxide concentration is calculated for each model grid.

The source MOZART data files are in netCDF format, which can be obtained from NCAR (https://www.acom.ucar.edu/wrf-chem/mozart.shtml).

3.3.12 SPRINTARS

The vertical profile of aerosol mass mixing ratio using the aerosol transport model

SPRINTARS. The calculation is performed in NIES.

3.3.13 MODIS L3 MYD11A1

Surface emissivity data from MODIS/Aqua.

MYD11A1 data files are in HDF-EOS format and can be obtained from USGS (https://e4ftl01.cr.usgs.gov/MOLA/MYD11A1.006/).

3.3.14 MODIS L3 MCD12Q1

Land cover data from MODIS/Terra and MODIS/Aqua.

MCD12Q1 data files are in HDF-EOS format and can be obtained from USGS (https://e4ftl01.cr.usgs.gov/MOTA/MCD12Q1.006/).

3.3.15 MODIS L3 MYD13Q1

Normalized Difference Vegetation Index data from MODIS/Aqua.

MYD13Q1 data files are in HDF-EOS format and can be obtained from USGS (https://e4ftl01.cr.usgs.gov/MOLA/MYD13Q1.006/).

3.3.16 MODIS L3 MYD10C1

Snow cover data from MODIS/Aqua.

MYD10C1 data files are in HDF-EOS format and can be obtained from NSIDC (https://nsidc.org/data/MYD10C1).

3.3.17 MODIS L3 (SST)

Sea surface temperature data from MODIS/Aqua.

SST data files are in netCDF format and can be obtained from NASA PODAAC (https://podaac-tools.jpl.nasa.gov/drive/files/allData/modis/L3/aqua/).

3.3.18 MODIS L3 MYD29P1D/1N

Sea ice data from MODIS/Aqua.

MYD29P1D/1N data files are in HDF-EOS format and can be obtained from NSIDC (https://nsidc.org/data/myd29p1d/, https://nsidc.org/data/myd29p1n/).

3.3.19 NOAA OISST (AVHRR-Only)

Sea surface temperature data which are interpolated based on sea surface temperature data from satellites, ships, buoys, etc., and released by NOAA.

OISST (AVHRR-Only) data files are in netCDF format and can be obtained from NOAA

(https://www.ncei.noaa.gov/data/sea-surface-temperature-optimum-interpolation/v2.1/access/avhrr/).

3.3.20 NSIDC Data Set ID: G02135

Sea ice index data from SSMIS/DMSP.

G02135 data files are in GeoTIFF format and can be obtained from NSIDC (ftp://sidads.colorado.edu/DATASETS/NOAA/G02135/).

3.3.21 NSIDC Data Set ID: NISE

Snow and ice data from SSMIS/DMSP.

NISE data files are in HDF-EOS format and can be obtained from NSIDC (https://n5eil01u.ecs.nsidc.org/OTHR/NISE.005/).

3.3.22 CAI-2 L1B Product

TANSO-CAI-2 L1B Product observed in the same day and same orbit as TANSO-FTS-2.

TANSO-CAI-2 L1B Product is in HDF5 file format and can be obtained from GOSAT-2 Product Archive (https://prdct.gosat-2.nies.go.jp/).

3.3.23 Result of CAI-2 L2 pre-processing (surface albedo)

Surface albedo data calculated using TANSO-CAI-2 L1B Product for approximately one month before and after the observation date for the same path as observed by TANSO-FTS-2. For details, see “GOSAT-2 TANSO-CAI-2 L2 Pre-processing Algorithm Theoretical Basis Document”.

3.3.24 CAI-2 L2 Cloud Discrimination Product

TANSO-CAI-2 L2 Cloud Discrimination Product observed in the same orbit as TANSO-FTS-2.

TANSO-CAI-2 L2 Cloud Discrimination is in HDF5 file format and can be obtained from GOSAT-2 Product Archive (https://prdct.gosat-2.nies.go.jp/).

3.3.25 CAI-2 L2 Aerosol Property Product

TANSO-CAI-2 L2 Aerosol Property Product observed in the same orbit as TANSO-FTS-2.

TANSO-CAI-2 L2 Aerosol Property Product is in HDF5 file format and can be obtained from GOSAT-2 Product Archive (https://prdct.gosat-2.nies.go.jp/).

4. FTS-2 L2 Pre-processing Algorithm

4.1 Overview of Algorithm

Figure 4.1-1 shows an overview flow of FTS-2 L2 pre-processing algorithm.

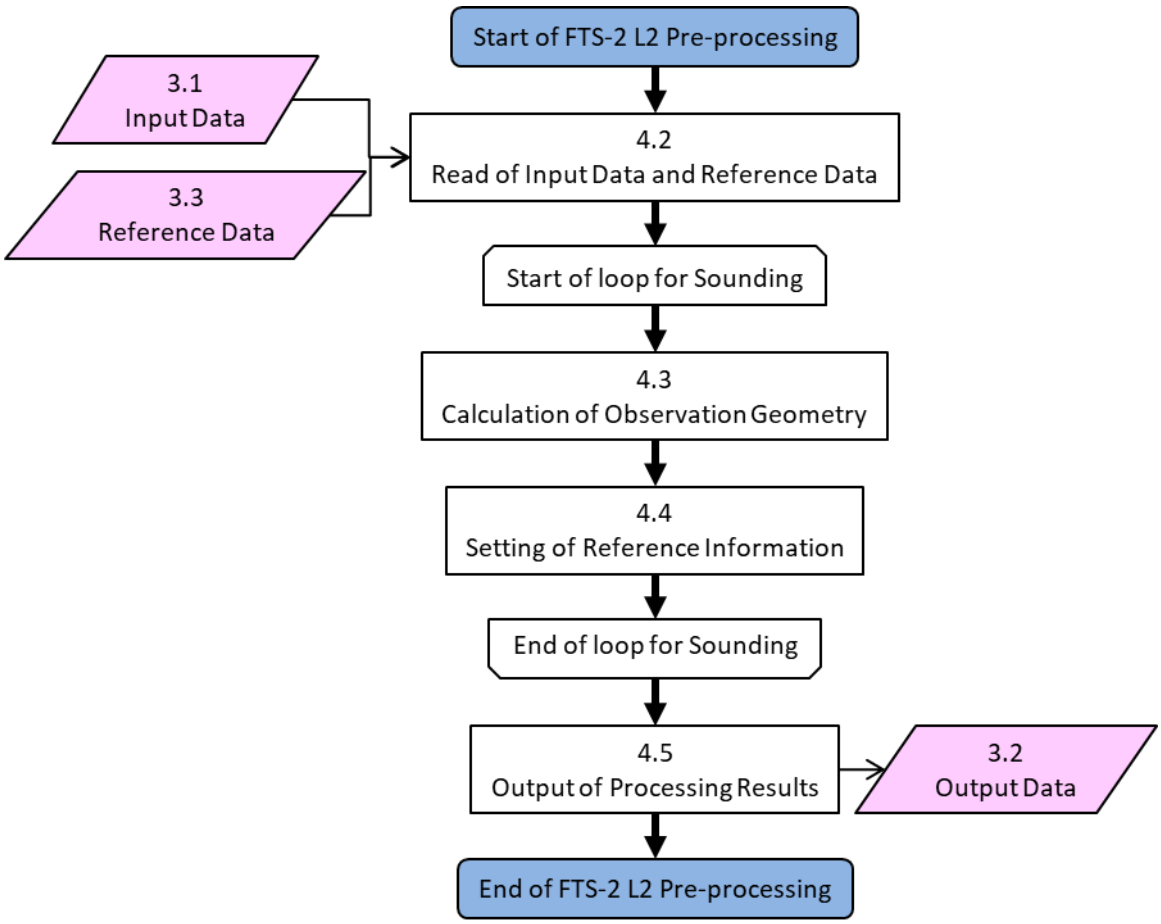

Figure 4.1-1. Overview flow of FTS-2 L2 pre-processing.

4.2 Read of Input Data and Reference Data

The input data shown in Section 3.1 (FTS-2 L1B Product) and the reference data shown in Section 3.3 are read out.

4.3 Calculation of Observation Geometry

The observation point stored in FTS-2 L1B Product is a position on the surface of an ellipsoidal earth. In this section, the center of the FTS-2 IFOV, the IFOV-area, and the extended IFOV-area with a margin added to the IFOV are calculated by considering the topography. The FTS-2 extended IFOV-area is for considering the possibility that clouds may flow into the FTS-2 IFOV due to the difference in the observation time when using the CAI-2 data observed at a

different viewing angle from FTS-2.

Furthermore, the following information which are used for a forward model calculation in the FTS-2 L2 processing are calculated: solar zenith and azimuth angle, satellite zenith and azimuth angle, and angle between direction of specular reflection and viewing direction with respect to the center of the FTS-2 IFOV; angle between radiative transfer reference plane and FTS-2 scan mirror reflection reference plane; incident angle to FTS-2 scan mirror; angle between FTS-2 scan mirror reflection reference plane and FTS-2 detector reference plane; angle between polarization plane of observation light and radiative transfer reference plane; and Doppler velocity for the sun and the satellite from the center of the FTS-2 IFOV.

4.3.1 Center of FTS-2 IFOV

The intersection of the ground surface and the viewing vector considering topography is obtained by using the satellite position (ECR) at the FTS-2 observation time, the viewing vector (satellite coordinate system), and the coordinate transformation matrix from satellite coordinate system to ECR coordinate system, which are stored in FTS-2 L1B Product (i.e., Ortho correction).

This processing uses the same algorithm as CAI-2 L1B processing. For details, see "GOSAT-2 TANSO-CAI-2 L1B Processing Algorithm Theoretical Basis Document". The topographical information is provided by digital elevation model data (Subsection 3.3.1) and geoid height data (Subsection 3.3.2).

4.3.2 FTS-2 IFOV-area and extended IFOV-area

The FTS-2 IFOV-area can be expressed as the intersections of a group of conical vectors, spreading in (IFOV / 2 + $\delta\theta$) (= 15.8 mrad / 2 + $\delta\theta$ = 7.9 mrad + $\delta\theta$) steradian around the viewing vector, with the earth's surface. $\delta\theta$ is the margin angle for the IFOV. It is expressed as 0 mrad when calculating the IFOV-area and as 2 mrad when calculating the extended IFOV-area. In this processing, 36 polygons approximate this cone with 10˚ intervals. Thus, the FTS-2 IFOV-area is approximated by 36 polygons.

The group of vectors $\mathbf{E}_{S,i}$ (i = 1 to 36) (satellite coordinate system) spreading in (IFOV / 2 + $\delta\theta$) steradian around the viewing vector is expressed by the following equation. The intersection of the ground surface is obtained in the same way as Subsection 4.3.1. $\mathbf{A}$, θ_{AT}, θ_{CT} are, respectively, the coordinate transformation matrix from the TANSO-FTS-2 optical axis coordinate to the satellite coordinate, the motor rotation angle around AT and CT axis at the observation time, which are stored in FTS-2 L1B Product. Unless otherwise noted, the unit of angle is recognized as already converted to radian.

$$\mathbf{E}_{S,i} = \mathbf{A} \cdot \left[-\mathbf{u}_i + 2(\mathbf{u}_i \cdot \mathbf{n}_{PM})\mathbf{n}_{PM} \right] \qquad (4.3.2\text{-}1)$$

$$\mathbf{n}_{PM} = \begin{pmatrix} n_{PM,x} & n_{PM,y} & n_{PM,z} \end{pmatrix}^T = \mathbf{L}_{AT} \cdot \mathbf{L}_{CT} \cdot \mathbf{n}_{PM,0} \tag{4.3.2-2}$$

$$\mathbf{E}_{S,i} = \begin{pmatrix} E_{Sx,i} \\ E_{Sy,i} \\ E_{Sz,i} \end{pmatrix} \tag{4.3.2-3}$$

$$\mathbf{A} = \begin{pmatrix} A_{11} & A_{12} & A_{13} \\ A_{21} & A_{22} & A_{23} \\ A_{31} & A_{32} & A_{33} \end{pmatrix} \tag{4.3.2-4}$$

$$\mathbf{L}_{AT} = \begin{pmatrix} \cos\theta_{AT} & 0 & \sin\theta_{AT} \\ 0 & 1 & 0 \\ -\sin\theta_{AT} & 0 & \cos\theta_{AT} \end{pmatrix} \tag{4.3.2-5}$$

$$\mathbf{L}_{CT} = \begin{pmatrix} 1 & 0 & 0 \\ 0 & \cos\theta_{CT} & -\sin\theta_{CT} \\ 0 & \sin\theta_{CT} & \cos\theta_{CT} \end{pmatrix} \tag{4.3.2-6}$$

$$\mathbf{n}_{PM,0} = \begin{pmatrix} \frac{1}{\sqrt{2}} & 0 & \frac{1}{\sqrt{2}} \end{pmatrix}^T \tag{4.3.2-7}$$

$$\mathbf{u}_i = \begin{pmatrix} \cos\left(\frac{IFOV}{2} + \delta\theta\right) \\ \sin\left(\frac{IFOV}{2} + \delta\theta\right)\cos\frac{i\pi}{18} \\ \sin\left(\frac{IFOV}{2} + \delta\theta\right)\sin\frac{i\pi}{18} \end{pmatrix} \tag{4.3.2-8}$$

4.3.3 Zenith angle, azimuth angle, and angle between direction of specular reflection and viewing direction

The zenith angle, azimuth angle, and angle between direction of specular reflection and viewing direction are calculated by using the apparent solar position (ECR) and satellite position (ECR) stored in FTS-2 L1B Product, and the center of the FTS-2 IFOV (geodetic coordinate system) obtained in Subsection 4.3.1, in the following manner.

(1) Convert the center of the FTS-2 IFOV in geodetic coordinate system to ECR coordinate system.

(2) Calculate the vector from the center of the FTS-2 IFOV (ECR) to the apparent solar position (ECR) or the satellite position (ECR).

(3) Convert the vector obtained in (2) to polar coordinate system at the center of the FTS-2 IFOV

(geodetic coordinate system). The zenith angle and azimuth angle obtained here are the necessary angles.

(4) Calculate the angle between direction of specular reflection and viewing direction, which is called Cone Angle in "GOSAT-2 TANSO-CAI-2 L2 Cloud Discrimination Processing Algorithm Theoretical Basis Document", by using the solar zenith and azimuth angle, and satellite zenith and azimuth angle obtained in (3).

<Conversion from geodetic coordinate system to ECR coordinate system>

The geodetic coordinate system (latitude φ, longitude λ, ellipsoidal height H) and ECR coordinate system (ECR_x, ECR_y, ECR_z) are related by Eq. (4.3.3-1). a, e, f are, respectively, the semi-major axis, eccentricity, and oblateness of the ellipsoidal earth.

$$\begin{cases} ECR_x = (N+H)\cos\varphi\cos\lambda \\ ECR_y = (N+H)\cos\varphi\sin\lambda \\ ECR_z = \{(1-e^2)N+H\}\sin\varphi \end{cases} \quad (4.3.3\text{-}1)$$

$$N = \frac{a}{\sqrt{1-e^2\sin^2\varphi}} \quad (4.3.3\text{-}2)$$

$$e^2 = f\cdot(2-f) \quad (4.3.3\text{-}3)$$

<Conversion from ECR coordinate system to polar coordinate system>

With the ECR notation of the unit vectors, **e**, **n**, and **u,** of the east, north, and zenith directions in the geodetic coordinate system (latitude φ, longitude λ), an arbitrary vector (ECR) can be decomposed into these components.

$$\begin{pmatrix} ECR_e \\ ECR_n \\ ECR_u \end{pmatrix} = \begin{pmatrix} -\sin\lambda & \cos\lambda & 0 \\ -\cos\lambda\sin\varphi & -\sin\lambda\sin\varphi & \cos\varphi \\ \cos\lambda\cos\varphi & \sin\lambda\cos\varphi & \sin\varphi \end{pmatrix} \begin{pmatrix} ECR_x \\ ECR_y \\ ECR_z \end{pmatrix} \quad (4.3.3\text{-}4)$$

Thus, the conversion to polar coordinate system (r, θ, ϕ) is expressed as Eq. (4.3.3-5) (see Figure 4.3.3-1). θ and ϕ are the zenith and azimuth angle to be obtained respectively. As shown in the figure, the azimuth angle is defined as a starting point in the north (0 degree) and a positive angle in the clockwise direction (90 degrees in the east).

$$\begin{pmatrix} r \\ \theta \\ \phi \end{pmatrix} = \begin{pmatrix} \sqrt{ECR_e^2 + ECR_n^2 + ECR_u^2} \\ \frac{\pi}{2} - \tan^{-1} \frac{ECR_u}{\sqrt{ECR_e^2 + ECR_n^2}} \\ \tan^{-1} \frac{ECR_e}{ECR_n} \end{pmatrix} \quad (4.3.3\text{-}5)$$

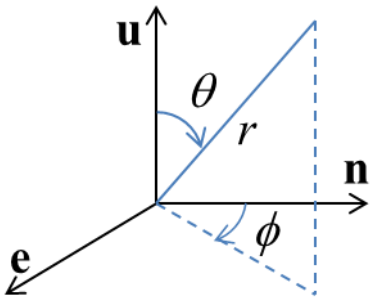

Figure 4.3.3-1. Conversion to polar coordinate system.

<Angle between direction of specular reflection and viewing direction>

The angle between direction of specular reflection and viewing direction θ_{CONE} is obtained by Eq. (4.3.3-6). θ_0, ϕ_0, θ_1, ϕ_1 are, respectively, the solar zenith angle, solar azimuth angle, satellite zenith angle, and satellite azimuth angle obtained above.

$$\theta_{CONE} = \cos^{-1}\left[\cos\theta_0 \cos\theta_1 - \sin\theta_0 \sin\theta_1 \cos(\phi_0 - \phi_1)\right] \quad (4.3.3\text{-}6)$$

4.3.4 Angle between radiative transfer reference plane and FTS-2 scan mirror reflection reference plane

The radiative transfer reference plane is a plane containing the vector from the observation point to the zenith direction and the vector from the observation point to the satellite. However, if the satellite is at the zenith, the reference plane contains the vector from the observation point to the zenith direction and the vector from the observation point to the sun. On the other hand, the FTS-2 scan mirror reflection reference plane is a plane containing incident light and reflected light for the FTS-2 scan mirror. The direction of the light reflected by the FTS-2 scan mirror is always constant in the satellite coordinate system.

(1) Convert the vector $\mathbf{r} = (1,0,0)^T$ representing the direction of the reflected light from the FTS-2

scan mirror using the coordinate transformation matrix from FTS-2 optical coordinate system to satellite coordinate system and from satellite coordinate system to ECR coordinate system which are stored in FTS-2 L1B Product. Furthermore, convert the vector to polar coordinate system at the center of the FTS-2 IFOV (geodetic coordinate system) (See Subsection 4.3.3).

(2) Calculate the angle between the radiative transfer reference plane and the FTS-2 scan mirror reflection reference plane by the spherical trigonometry (See Figure 4.3.4-1).

$$\theta_{RT-PM} = \cos^{-1}\left(\frac{\cos\theta_2 - \cos\theta_1\cos\Theta}{\sqrt{1-\cos^2\Theta}\sqrt{1-\cos^2\theta_1}}\right) \quad (4.3.4\text{-}1)$$

$$\cos\Theta = \cos\theta_1\cos\theta_2 + \sin\theta_1\sin\theta_2\cos(\phi_1 - \phi_2) \quad (4.3.4\text{-}2)$$

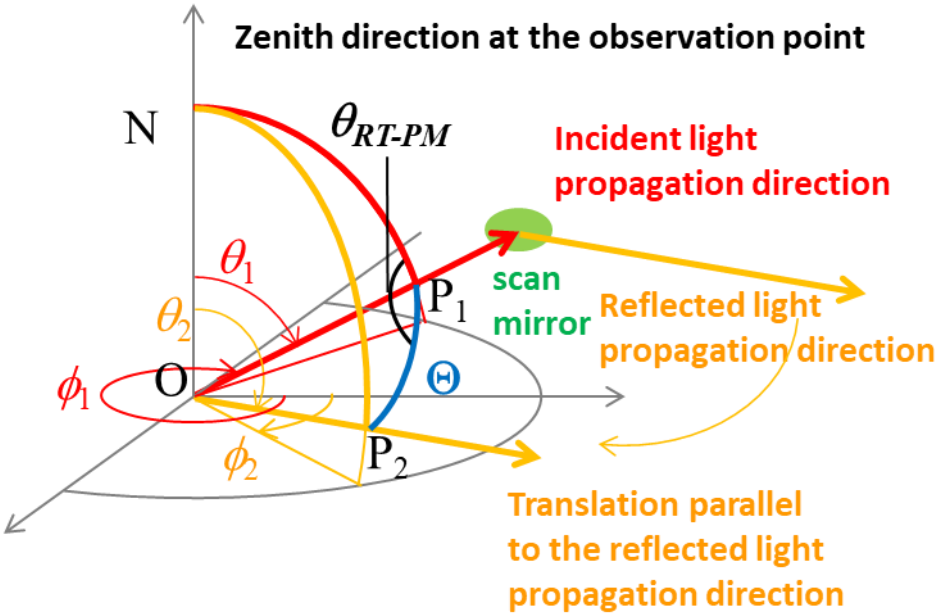

Figure 4.3.4-1. Angle between radiative transfer reference plane (NOP_1) and FTS-2 scan mirror reflection reference plane (P_1OP_2), $\theta_{RT\text{-}PM}$.

4.3.5 Incident angle to scan mirror and angle between FTS-2 scan mirror reflection reference plane and FTS-2 detector reference plane

The incident angle on the FTS-2 scan mirror can be calculated from the inner product of the vector representing the direction of the reflected light and the normal vector of the scan mirror since the incident angle is equal to the reflection angle. The cross product of these vectors is the normal vector of the FTS-2 scan mirror reflection reference plane. The angle between the FTS-2 scan mirror reflection reference plane and the FTS-2 detector reference plane can be calculated from the

inner product of their normal vectors since the FTS-2 detector reference plane is the X-Z plane of the satellite coordinate system (to the X-axis direction of reflected light, the component in Z-axis direction is P-polarization and the component in Y-axis direction is S-polarization.).

The normal vector of the FTS-2 scan mirror $\mathbf{n}_{PM}$ is given by Eq. (4.3.2-2). Thus, the incident angle on the FTS-2 scan mirror θ_{in} is

$$\begin{aligned}\theta_{in} &= \cos^{-1}\left(\mathbf{r}\cdot\mathbf{n}_{PM}\right)\\ &= \cos^{-1}\left(n_{PM,x}\right)\end{aligned} \tag{4.3.5-1}$$

The angle between the FTS-2 scan mirror reflection reference plane and the FTS-2 detector reference plane $\theta_{PM\text{-}DET}$ is

$$\begin{aligned}\theta_{PM-DET} &= \cos^{-1}\left\{\left(\frac{\mathbf{r}\times\mathbf{n}_{PM}}{\left|\mathbf{r}\times\mathbf{n}_{PM}\right|}\right)\cdot\begin{pmatrix}0 & 1 & 0\end{pmatrix}^{T}\right\}\\ &= \cos^{-1}\left(\frac{n_{PM,z}}{\sqrt{1-n_{PM,x}^{2}}}\right)\end{aligned} \tag{4.3.5-2}$$

4.3.6 Angle between polarization plane of observation light and radiative transfer reference plane

As shown in Figure 4.3.6-1, the angle between the polarization plane of observation light and radiative transfer reference plane χ_{ss} is calculated by the spherical trigonometry. θ_0, ϕ_0, θ_1, ϕ_1 are the solar zenith angle, solar azimuth angle, satellite zenith angle, and satellite azimuth angle, which are obtained in Subsection 4.3.3, respectively.

$$\chi_{ss} = \cos^{-1}\left(\frac{\cos\theta_0 + \cos\theta_1\cos\Theta}{\sqrt{1-\cos^2\Theta}\sqrt{1-\cos^2\theta_1}}\right) \tag{4.3.6-1}$$

$$\cos\Theta = -\cos\theta_0\cos\theta_1 + \sin\theta_0\sin\theta_1\cos\left(\phi_0 - \phi_1 + \pi\right) \tag{4.3.6-2}$$

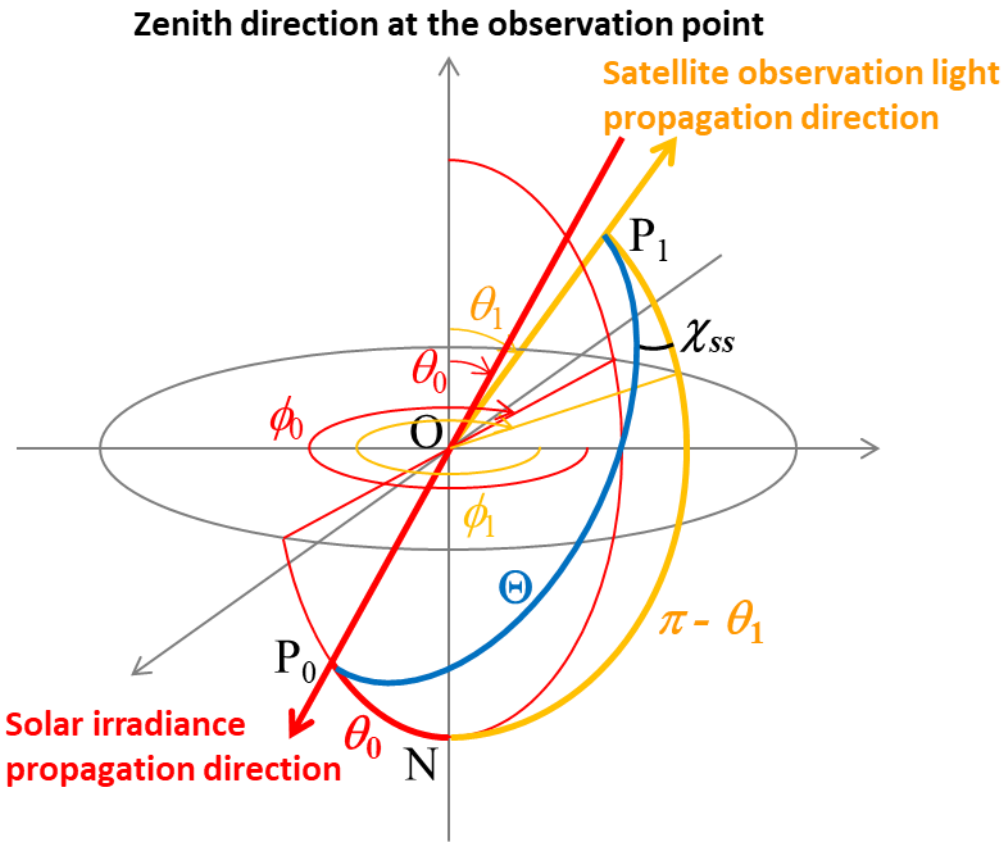

Figure 4.3.6-1. Angle between polarization plane of observation light (P_0OP_1) and radiative transfer reference plane (NOP_1), χ_{ss}.

4.3.7 Doppler velocity

The Doppler velocity from the center of the FTS-2 IFOV is calculated by using the solar position (ECR), solar velocity (ECR), satellite position (ECR), and satellite velocity (ECR), which are stored in FTS-2 L1B Product, and the center of the FTS-2 IFOV (ECR) obtained above, in the following manner. In this case, the Doppler velocity when approaching each other is positive.

(1) Calculate unit vector from the solar position (ECR) or the satellite position (ECR) to the center of the FTS-2 IFOV (ECR).

(2) Calculate the radial component of the velocity by taking the inner product of the unit vector obtained in (1) and the solar velocity (ECR) or satellite velocity (ECR).

$$v_{dop} = \frac{\mathbf{v}_{target} \cdot \left(\mathbf{E}_{obs} - \mathbf{E}_{target}\right)}{\left|\mathbf{E}_{obs} - \mathbf{E}_{target}\right|} \qquad (4.3.7\text{-}1)$$

where $\mathbf{E}_{obs}$ is the center of the FTS-2 IFOV (ECR), and $\mathbf{E}_{target}$ and $\mathbf{v}_{target}$ are respectively the position (ECR) and velocity (ECR) of the sun or the satellite.

4.4 Setting of Reference Information

Reference information used in FTS-2 L2 processing, such as atmospheric data, gas concentration data, surface data, and cloud condition within FTS-2 IFOV, should be prepared. The reference information includes not only physical quantities but also category information such as land-sea masks and land cover classifications. The setting method and/or setting contents differ depending on the spatial resolution or type of reference information to be used. Table 4.4-1 shows the processing categories for each reference information data. If the corresponding information does not exist, invalid values should be set.

(a) In the case that the spatial resolution of the reference information is sufficiently smaller than the FTS-2 IFOV-area.

In this case, the FTS-2 IFOV-area contains multiple (generally dozens to hundreds) pieces of reference information data. If the reference information data are physical quantities, the average, standard deviation, and mode of valid reference information data included in the FTS-2 IFOV-area are calculated. Furthermore, time interpolation is performed as needed. If the reference information is category information, the frequency by category is aggregated.

(b) In the case that the spatial resolution of the reference information is sufficiently larger than the FTS-2 IFOV-area.

In this case, the FTS-2 IFOV-area does not necessarily contain reference information data. Therefore, the reference information data are interpolated in time and space to the FTS-2 observation time and the center of the IFOV-area, or nearest neighbor grid data are extracted.

The spatiotemporal interpolation is a linear interpolation for time or latitude and longitude (Eq. 4.4-1).

For this interpolation, the FTS-2 observation time stored in FTS-2 L1B Product or the reference information data adjacent to the center of the FTS-2 IFOV obtained in Subsection 4.3.1. In this case, the number of layers in the vertical profile is based on the source data.

$$x(s)=\left(\frac{s_1-s}{s_1-s_0}\right)x(s_0)+\left(\frac{s-s_0}{s_1-s_0}\right)x(s_1) \qquad (4.4\text{-}1)$$

where s is either the FTS-2 observation time or the latitude and longitude of the center of the FTS-2 IFOV, s_0 and s_1 are the nearest grid satisfying $s_0 \le s \le s_1$, and x is the reference information data to be interpolated

As for the specific humidity data of the JRA-55 model level analysis fields data, the value 9.9999956E-13 [kg/kg] is treated as an invalid value. If the vertical profile of the specific humidity of the grid used for the spatiotemporal interpolation contains an invalid value, replace it with a value linearly interpolated with respect to the pressure using the valid upper and lower specific humidity values closest to the invalid data. The aforementioned spatiotemporal interpolation is conducted after replacing the invalid specific humidity values. If the specific humidity value of the lowest layer of the JRA-55 model level analysis fields data is the invalid value, the value to be replaced is obtained by linear interpolation of the pressure using the lowest valid specific humidity value of the JRA-55 model level analysis fields data and the specific humidity value of the JRA-55 surface analysis fields data.

Also, the surface pressure and surface temperature are derived by vertical inter-/extra-polation of the spatiotemporal interpolated JRA-55 model level analysis fields data at the average elevation within the FTS-2 IFOV-area rather than the spatiotemporal interpolation of the JRA-55 surface analysis fields data. In the case that the average elevation within the FTS-2 IFOV-area is lower than the geopotential height of the lowest level of the JRA-55 model level analysis fields data, the surface pressure is obtained by linear extrapolation of the logarithm of the pressure using the geopotential heights of the lowermost two levels of the JRA-55 model level analysis fields data. Also, the surface temperature is obtained by extrapolation with an assumption of temperature lapse rate of -5 K/km as elevation increases. In the case that the average elevation within the FTS-2 IFOV-area is higher than the geopotential height of the lowest level of the JRA-55 model level analysis fields data, the surface pressure and the surface temperature are obtained by the spline interpolation of the logarithm of the pressure profile and temperature profile in the vertical direction, respectively. 02

Table 4.4-1. Processing category for reference information data.

Reference data	FTS-2	Time	Space
Digital elevation model data	IFOV-area	N/A	Average/standard deviation/mode
Global land/sea flag	IFOV-area	N/A	Category aggregation
JRA-55	Center of IFOV	Interpolation	Interpolation
Variance-covariance matrix (JRA-55)	Center of IFOV	Interpolation	Nearest neighbor
NICAM-TM	Center of IFOV	Interpolation	Interpolation

02

Reference data	FTS-2	Time	Space
Variance-covariance matrix (NCIAM-TM)	Center of IFOV	Interpolation	Nearest neighbor
ACTM	Center of IFOV	Interpolation	Interpolation
Variance-covariance matrix (ACTM)	Center of IFOV	Interpolation	Nearest neighbor
CO climatological value (concentration profile)	Center of IFOV	Interpolation	Interpolation
Variance-covariance matrix (CO climatological value)	Center of IFOV	Interpolation	Nearest neighbor
SPRINTARS	Center of IFOV	Interpolation	Interpolation
MODIS L3 MYD11A1	IFOV-area	Nearest neighbor	Average/standard deviation/mode
MODIS L3 MCD12Q1	IFOV-area	Nearest neighbor	Category aggregation
MODIS L3 MYD13Q1	IFOV-area	Nearest neighbor	Average/standard deviation/mode
MODIS L3 MYD10C1	IFOV-area	Nearest neighbor	Average/standard deviation/mode
MODIS L3 (SST)	IFOV-area	Nearest neighbor	Average/standard deviation/mode
MODIS L3 MYD29P1D/1N	IFOV-area	Nearest neighbor	Average/standard deviation/mode Category aggregation
NOAA OISST (AVHRR-Only)	Center of IFOV	Same day	Interpolation
NSIDC Data Set ID: G02135	Center of IFOV	Same day	Interpolation (physical quantities) Nearest neighbor (category information)
NSIDC Data Set ID: NISE	Center of IFOV	Same day	Interpolation (physical quantities) Nearest neighbor (category information)

Reference data	FTS-2	Time	Space
CAI-2 L1B Product [1)]	Extended IFOV-area	Same path	Average/standard deviation/mode
CAI-2 NDVI [1) 2)]	IFOV-area	Same path	Average/standard deviation/mode
CAI-2 L2 Cloud Discrimination Product [1)]	Extended IFOV-area	Same path	Category aggregation
CAI-2 L2 Aerosol Property Product [1)]	IFOV area	Same path	Average/standard deviation/mode

1) Set only for day side observation.

2) CAI-2 NDVI is calculated from CAI-2 L2 pre-processing results (surface albedo). See Subsection 4.4.3.

4.4.1 Calculation of tropopause height

The tropopause height is calculated by using atmospheric data interpolated in the center of the FTS-2 IFOV by the following two methods.

<Temperature lapse rate method>

If the height range where the temperature lapse rate is 2 K/km continues for 1 km or more within the range of the geopotential height at 500 hPa to 50 hPa, the lowest altitude is defined as the tropopause height (temperature lapse rate method). If the above condition is not satisfied, the 200 hPa geopotential height is defined as the tropopause height (temperature lapse rate method).

In the actual processing, the condition is determined by calculating the temperature lapse rate with the temperature profile which is spline interpolated with 10 m intervals.

<Minimum temperature method>

Within the range of the geopotential height at 500 hPa to 50 hPa, the altitude whose temperature is the lowest is defined as the tropopause height (minimum temperature method).

In the actual processing, the condition is determined by the temperature profile which is spline interpolated with 0.1 hPa intervals.

4.4.2 Calculation of gravity

Gravity is calculated by using the latitude and geopotential height interpolated in the center of the FTS-2 IFOV.

Gravitational potential U is expressed by Eq. (4.4.2-1) by using the distance from the center of the earth r and the polar angle θ.

$$U(r,\theta) = -\frac{GM}{r}\left[1 - J_2\left(\frac{a}{r}\right)^2\left(\frac{3}{2}\cos^2\theta - \frac{1}{2}\right)\right] - \frac{1}{2}r^2\omega^2\sin^2\theta \tag{4.4.2-1}$$

where a is the equatorial radius of the earth, GM is the gravitational constant, ω is the angular velocity of the earth, and J_2 is the second order coefficient in the spherical harmonic expansion.

The vertically downward gravity g at any ellipsoidal height H is expressed by Eq. (4.4.2-2) by using H and φ instead of r and θ as an independent variable (Figure 4.4.2-1).

$$g = -g_H = \frac{\partial U(H,\varphi)}{\partial H} = -g_r\cos(\varphi - \phi) + g_\theta\sin(\varphi - \phi) \tag{4.4.2-2}$$

$$g_r = -\frac{\partial U(r,\theta)}{\partial r} = -\frac{GM}{r^2}\left[1 - 3J_2\left(\frac{a}{r}\right)^2\left(\frac{3}{2}\cos^2\theta - \frac{1}{2}\right)\right] + r\omega^2\sin^2\theta \tag{4.4.2-3}$$

$$g_\theta = -\frac{1}{r}\frac{\partial U(r,\theta)}{\partial\theta} = \frac{GM}{r^2}3J_2\left(\frac{a}{r}\right)^2\sin\theta\cos\theta + r\omega^2\sin\theta\cos\theta \tag{4.4.2-4}$$

$$r = \sqrt{X^2 + Z^2} \tag{4.4.2-5}$$

$$X = (N + H)\cos\varphi \tag{4.4.2-6}$$

$$Z = \left[N(1 - e^2) + H\right]\sin\varphi \tag{4.4.2-7}$$

$$\phi = \tan^{-1}\frac{Z}{X} \tag{4.4.2-8}$$

For N and e, see Eqs. (4.3.3-2) and (4.3.3-3).

Since the geopotential height z is expressed by Eq. (4.4.2-9) by using the geopotential and the standard gravity acceleration g_0, the vertically downward gravity corresponding to the geopotential height of each layer can be numerically obtained.

$$z = \frac{U(r,\theta)}{g_0} \tag{4.4.2-9}$$

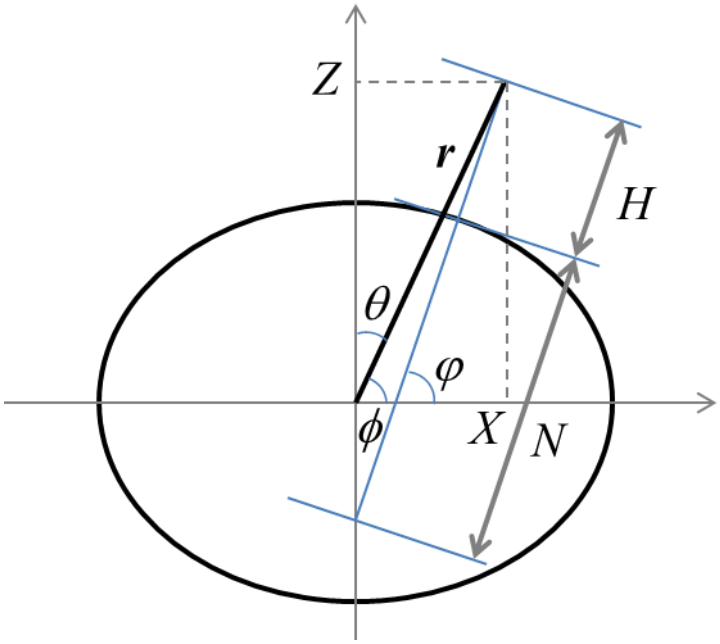

Figure 4.4.2-1. Ellipsoidal earth.

4.4.3 CAI-2 NDVI (only for the day side observation)

CAI-2 NDVI for each viewing direction is calculated by using CAI-2 surface albedo A_g which is calculated in CAI-2 L2 pre-processing. For the calculation method of A_g, see "GOSAT-2 TANSO-CAI-2 L2 Pre-processing Algorithm Theoretical Basis Document".

$$NDVI_{CAI-2,FWD/BWD} = \frac{A_{g,BAND4/9} - A_{g,BAND3/8}}{A_{g,BAND4/9} + A_{g,BAND3/8}} \quad (4.4.3\text{-}1)$$

where the subscripts FWD/BWD represent the viewing directions of CAI-2, and are calculated by using Bands 3 and 4, and Bands 8 and 9, respectively.

The average, standard deviation, and mode within the FTS-2 IFOV-area of the CAI-2 NDVI obtained by Eq. (4.4.3-1) are calculated for each CAI-2 viewing direction.

4.4.4 CAI-2 cloud determination (only for the day side observation)

Based on the CAI-2 information, the presence of clouds within the extended FTS-2 IFOV-area is determined. This subsection describes each determination method. How to combine these determination results in subsequent processing is described in each Algorithm Theoretical Basis Document.

<CAI-2 L2 Cloud Discrimination Product>

The cloud determination within the extended FTS-2 IFOV-area is performed by using CAI-2 L2 Cloud Discrimination Product. The overall clear confidence level Q is provided to each pixel and each viewing direction of CAI-2 in CAI-2 L2 Cloud Discrimination Product.

In FTS-2 L2 pre-processing, the overall clear confidence level Q of each pixel of CAI-2 L2 Cloud Discrimination Product within the extended FTS-2 IFOV-area is classified into 16 levels, which is the same as the bit field of cloud status bit data. Then, the number of pixels is aggregated by viewing direction and range ($N_{CLDD,FWD/BWD,i}$; i = 0－15). If Eq. (4.4.4-1) is satisfied, it is determined that clouds are present in the extended FTS-2 IFOV-area. Table 4.4.4-1 shows the parameter M_{CLDD} representing the range of the category to be integrated and the threshold VAL_{CLDD}.

$$\frac{\sum_{i=0}^{M_{CLDD}} N_{CLDD,FWD/BWD,i}}{N_{TOTAL,FWD/BWD}} > VAL_{CLDD} \qquad (4.4.4\text{-}1)$$

where $N_{TOTAL,\ FWD/BWD}$ is the total number of CAI-2 pixels for forward (FWD) and backward (BWD) viewing direction within the extended FTS-2 IFOV-area.

The determination results by Eq. (4.4.4-1) can be obtained for both CAI-2 forward and backward viewing direction. However, by considering that the accuracy of cloud discrimination on CAI-2 L2 Cloud Discrimination Product may deteriorate around sunglint areas over the ocean, the CAI-2 viewing direction used for the final cloud determination is as follows.

If CAI-2 pixels with low-accurate cloud discrimination are contained in the extended FTS-2 IFOV-area due to the influence of sunglint, the viewing direction with the smaller value by Eq. (4.4.4-2) is selected as the viewing direction with less influence. For the comparison, the index of Cone Angle range is used in order from the smallest Cone Angle value (i = 7) to $M_{CONE,\ max}$. The determination is made when a difference occurs in the value of Eq. (4.4.4-2).

$$\frac{N_{CONE,FWD/BWD,i}}{N_{TOTAL,FWD/BWD}} \qquad (4.4.4\text{-}2)$$

where $N_{CONE,\ FWD\ /\ BWD,\ i}$ (i = 0－7) is the number of CAI-2 ocean pixels for each viewing direction and each Cone Angle range, and uses the same category as the cloud status bit field. $M_{CONE,\ max}$ is the index of Cone Angle range including the maximum Cone Angle value where the accuracy of cloud discrimination is reduced due to the influence of sunglint.

In other cases, the viewing direction with the shortest difference between the observation time of CAI-2 pixel nearest to the center of the FTS-2 IFOV and the observation time of FTS-2 is

selected.

Table 4.4.4-1 Determination condition of cloud status within the extended FTS-2 IFOV-area with CAI-2 L2 Cloud Discrimination Product.

M_{CLDD}	VAL_{CLDD}	$M_{CONE,max}$
4 (Q < 0.34)	0.01	3 (Cone Angle < 35 deg.)

<CAI-2 L1B Product>

CAI-2 L2 Cloud Discrimination Product may not be able to detect CAI-2 sub-pixel size clouds. The presence of clouds in the extended FTS-2 IFOV-area is determined by using the average I_{AVG} and standard deviation I_{STD} of the radiance of each band of CAI-2 pixels included in the extended FTS-2 IFOV-area as an index. However, since the radiance of CAI-2 depends not only on the presence of clouds but also on the reflectance of the ground surface, this determination is intended for the sea area where the spatial uniformity of reflectance is relatively high; that is, I_{AVG} and I_{STD} are calculated only for CAI-2 pixels of the sea area. If Eq. (4.4.4-3) is satisfied, it is determined that clouds are present in the extended FTS-2 IFOV-area. CAI-2 Bands 1 and 6 which are less affected by the ground surface are used for the calculation.

$$\frac{I_{STD,i} + OFFSET_i}{I_{AVG,i}} > VAL_{COHERENT,i} \qquad (4.4.4\text{-}3)$$

where i is CAI-2 Band. For the values of $OFFSET$ and $VAL_{COHERENT}$, see Table 4.4.4-2.

The determination results by Eq. (4.4.4-3) can be obtained for both CAI-2 forward and backward viewing direction. However, by considering the ratio of the number of CAI-2 land pixels to the total number of CAI-2 pixels included in the extended FTS-2 IFOV-area (F_{LAND}), the CAI-2 viewing direction used for the final cloud determination is as follows.

If F_{LAND} in one of the forward and backward viewing direction is less than or equal to the threshold $F_{LAND,\ max}$, the viewing direction is selected. If F_{LAND} in both viewing directions are below the threshold, the viewing direction with the shortest difference between the observation time of the CAI-2 pixel nearest to the center of the FTS-2 IFOV and the observation time of FTS-2 is selected. If F_{LAND} in both viewing directions exceed the threshold, this is not applicable to this determination.

Table 4.4.4-2 Determination condition of cloud condition within the extended FTS-2 IFOV-area with CAI-2 L1B Product.

Band	$OFFSET$	$VAL_{COHERENT}$	$F_{LAND,max}$

1	-0.25	0.0020	0.0
6	-0.25	0.0035	

4.4.5 FTS-2 2 μm Band Cloud Determination (only for the day side observation)

The simple cloud determination is performed by using water vapor absorption bands in FTS-2 Band 3 (2 μm band). Since the observed radiance spectra of FTS-2 Band 3 are stored only in the SWIR file, this determination is performed only for the day side data.

The radiance of water vapor absorption band observed by the satellite for clear-sky areas is extremely low since water vapor is generally abundant in the lower atmosphere. If cloud or other scattering materials are present in the sky, the radiance observed by the satellite increases due to light scattering before being absorbed by water vapor. FTS-2 2 μm band cloud determination is based on this characteristic. This determination has high sensitivity in the upper atmosphere; therefore, it can detect optically thin cirrus clouds which are difficult to detect with CAI-2 L2 Cloud Discrimination Product. On the other hand, its low sensitivity to clouds in the lower atmosphere may cause overlooking them; however, if the clouds are optically thick, CAI-2 L2 Cloud Discrimination Product can detect them. They have a complementary relationship.

From the observed radiance spectra of FTS-2 Band 3 stored in FTS-2 L1B Product, the wavenumber channels with very strong absorption by water vapor are extracted, and the average and standard deviation of the radiance which are normalized with the noise level for each polarization component are obtained.

If either the average or standard deviation of the radiance normalized with the noise level is greater than the threshold, it is determined that clouds are present. The noise level is calculated from the observed radiance spectrum and SNR which are stored in FTS-2 L1B Product (Eq. 4.4.5-1). Table 4.4.5-1 shows the wavenumber range used in this calculation and Table 4.4.5-2 shows the thresholds.

The beginning wavenumber and wavenumber interval of the spectrum data stored in FTS-2 L1B Product are nominal values; therefore, some fluctuations are actually expected. The absorption line position of water vapor is affected by Doppler displacement according to the positional relationship between the satellite and observation point. However, in this case, it is assumed that the fluctuation range of the wavenumber axis due to these influences is sufficiently smaller than the wavenumber interval of the spectrum data, and the values stored in FTS-2 L1B Product are used.

$$NoiseLevel_{P/S} = \frac{Max(S_{P/S})}{SNR_{P/S}} \qquad (4.4.5\text{-}1)$$

where the subscript *P/S* is each polarization component, and *S* [V/cm^{-1}] is the observed

radiance spectrum. *Max(S)* is the maximum value of the observed radiance spectrum within the nominal wavenumber range.

Table 4.4.5-1. Wavenumber range used for FTS-2 2 μm band cloud determination.

Beginning wavenumber	Ending wavenumber
5184.4 cm^{-1}	5184.5 cm^{-1}
5188.6 cm^{-1}	5189.6 cm^{-1}
5196.4 cm^{-1}	5197.8 cm^{-1}

Table 4.4.5-2. Threshold used for FTS-2 2 μm band cloud determination.

	P-polarization component	S-polarization component
Average	1.5	1.5
Standard deviation	1.4	1.4

4.5 Output of Processing Results

Among the above processing results, those shown in the output data in Section 3.2 are output as files in HDF5 format.

5. Precondition and Restriction

When the source URL of reference data contains a version of each source data, the source data represents the version which was available in October 2020, not necessarily the version used for the processing (Section 3.3).

In FTS-2 L2 pre-processing, the FTS-2 IFOV is approximated by 36 polygons with 10° intervals (Subsection 4.3.2).

The cloud determination within the FTS-2 IFOV-area by using CAI-2 L1B Product is performed only when the land fraction within the extended FTS-2 IFOV-area is less than or equal to the threshold value. Other cases are treated as “not applicable” (Subsection 4.4.4).

In FTS-2 L2 pre-processing, the wavenumber axis is not corrected on the spectrum data stored in FTS-2 L1B Product (Subsection 4.4.5).

The coefficients and thresholds used in the cloud determination shown in Tables 4.4.4-1, 4.4.4-2, 4.4.5-1, and 4.4.5-2 are tentative values, and should be optimized based on the actual data after the satellite launch.

6. References

N/A.